11th International Conference on Green Energy & Environmental Engineering (GEEE-2025)
Proceedings of Engineering & Technology – PET-Vol 94, pp. 303-309

Impact of Crystallographic Directions on the Performance of $Ge/Ge_{1-x}Sn_x/Ge$ Quantum Wells for Mid-Infrared Detectors

Omar Zitouni[1,2], Nouha Mastour[1] and Said Ridene[1,*]
[1]Advanced Materials and Quantum Phenomena Laboratory, Physics Department, Faculty of Sciences of Tunis, University of Tunis El Manar, Tunis 2092, Tunisia; ozitouni555@gmail.com (O.Z.); mastournouha@yahoo.fr (N.M.)
[2]Laboratoire Photovoltaïque (LPV)- CRTEn Borj Cédria, Tunis, Tunisia

*****Correspondence: author. E-mail Address: said.ridene@fst.rnu.tn

Abstract: Band structure characteristics and optical gain of $Ge/Ge_{1-x}Sn_x/Ge$ quantum wells (QWs) are analyzed, focusing on the effects of Sn composition (x) and quantum well thickness, as well as the influence of crystallographic direction ([110] vs. [111]) on the material's optical properties. The study was conducted for different Sn fractions (x = 0.08 to 0.185) and QW thicknesses (8 nm to 14 nm), with a constant doping concentration of $N = 1.5 \times 10^{19}$ cm^{-3}. The optical gain was evaluated as a function of photon energy, revealing peaks in the infrared range (~0.45 to 0.6 eV). Additionally, a comparison of [110] and [111] directions highlighted anisotropic effects on the optical gain, with slight differences in energy and amplitude due to the material's crystallographic orientation.Furthermore, our work convincingly demonstrates that optimizing optical gain in such structures relies on fine control of confinement and composition parameters, and that the anisotropy associated with the [110] and [111] directions offers interesting prospects for polarization control and emission efficiency.

introduction

The ever-growing silicon-based microelectronics industry demands higher bandwidths for data exchange, reduced power consumption, and lower costs. Photonics integration presents numerous opportunities to address these challenges, with a focus on the development of passive devices (such as waveguides and couplers), active devices (like photodetectors and modulators), and integrated light sources. Most group IV semiconductors (such as carbon, silicon, and germanium) have an indirect bandgap in their bulk form, which prevents them from efficiently emitting light. The monolithic integration of direct bandgap III-V materials by epitaxy still faces challenges related to lattice mismatch and antiphase domain issues [1–3]. Although techniques such as nano-heteroepitaxy [4,5] and template-assisted selective epitaxy (TASE) [6,7] have been proposed to address these monolithic growth issues of III-V materials, they are still in the early stages and require further investigation to assess their effectiveness. Consequently, direct bonding of III-V heterostructures remains the preferred method for silicon-photonics integration.

Regarding germanium (Ge), despite its indirect bandgap, the energy separation between the Γ and L valleys is relatively small, only 140 meV. It is possible to lower the energy of the Γ valley below that of the L valley by applying uniaxial or biaxial tensile strain on the Ge layer [8–12] or by alloying Ge with Sn [13–14]. The latter approach has gained prominence since the 2015 demonstration of optically pumped lasing in a GeSn Fabry-Pérot optical cavity [13]. Follow-up studies have confirmed the stability of GeSn as a gain material and improved the performance of GeSn lasers by increasing Sn concentrations in the optically active layers and using electronic potential barriers made from low-Sn-content GeSn alloys. Based on these trends, it became essential to investigate the optical behavior of this type of alloy in crystallographic directions other than [001]. In this study, we report the hole subband states and optical

ISSN: 1737-9334

gain in [110] and [111]-oriented quantum wells. Indeed, for Ge/Ge1-xSnx/Ge alloys, only a few reports have focused on quantum wells grown in other crystallographic directions.

The purpose of this paper is to study the effect of the active zone width and the Sn concentration in the directions mentioned above on the band structure and optical gain.

The simultaneous presence of the [110] and [111] directions in our calculations revealed an anisotropy in the dispersion, indicating that the electronic response is directionally dependent. This anisotropy can be linked to strain effects and the symmetries of the lattice, particularly enhanced as the Sn composition increases.

Although both [110] and [111] orientations exhibit similar trends in terms of red-shift with increasing x, quantitative differences in the gain amplitude can be observed. This suggests that the intrinsic anisotropy of the crystal plays a role in optimizing optical transitions and can be exploited to modulate the device's polarized response.

The differences observed between these two directions highlight the importance of considering crystallographic anisotropy in modeling and fabrication. These effects could be exploited to adjust emission polarization or optimize interaction with specific optical cavities.

Finally, by keeping the carrier density constant, the study emphasizes the direct impact of geometric parameters on the gain behavior. This allows for the separation of effects related to quantum well engineering from doping effects, which is crucial for experimental design and result reproducibility.

Theoretical Approach to Optical Laser Gain in Ge/$Ge_{1-x}Sn_x$/Ge Quantum Wells

The analysis of optical gain properties, such as the injected carrier density and α-Sn concentration in the [110] and [111] crystallographic directions, requires an in-depth understanding of the subband structure. To this end, the conduction (CB) and valence (VB) subbands of Ge/Ge1−xSnx/Ge quantum wells will be explored using the 14-band k.p model, H [5, 9]. This model includes the k.p Hamiltonian, the deformation Hamiltonian, and the potential offsets associated with the VB and CB. In the [110] and [111] directions, this Hamiltonian has the same form as in references [5, 9], except for the modified Luttinger parameters, which must be replaced as indicated in table 1 of reference [2]. The band alignment scheme and the parameters for the CB and VB used in this approach are illustrated in Figure 1.

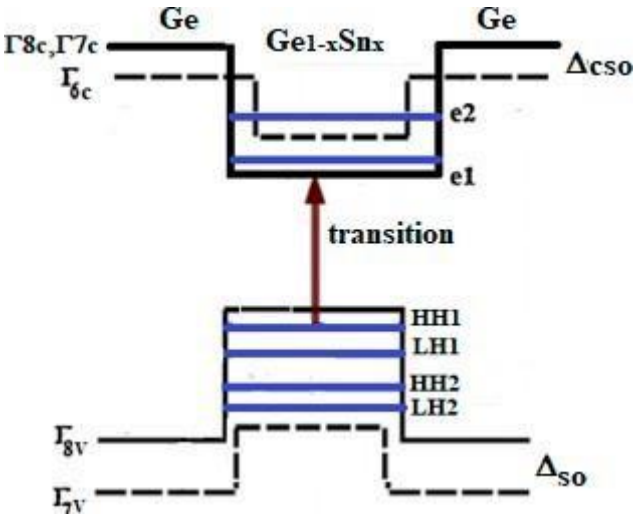

Figure 1. Band alignment structure of Ge/$Ge_{1-x}Sn_x$/Ge quantum wells. ΔSO and ΔCSO correspond to the spin-orbit splitting energies of the conduction band (CB) and valence band (VB), respectively.

To investigate the influence of the crystallographic direction, well width, and α-Sn concentration on the subband structure and optical gain, we have determined the dispersion relations for the CB and VB subbands of the Ge/Ge1−xSnx/Ge QWs as a function of these parameters. The values of the parameters for Ge and α-Sn used in the numerical calculations are provided in [2]. The well and barrier widths range from (8, 10) nm to 12 nm, while the confinement energy of the well is approximately 135 meV

ISSN: 1737-9334

for heavy-hole (HHn) and light-hole (LHn) states [10]. It should be noted that the energies are expressed in meV, with the energy reference chosen at the highest level of the unstrained HHn well. The numerical parameters for Ge and α-Sn used in this study are derived from references [19, 20]. Furthermore, the calculation of optical gain is based on the dependence of the subband structure for quantum wells (QWs), which is closely related to the 2D density of states (ρ2D), wavefunction overlap, intra-band relaxation time, quasi-Fermi levels, and the momentum matrix element of the optical transitions [11]:

$$g(\omega)=\frac{e^2}{m_0^2 n_r c\varepsilon_0\omega}\frac{1}{L_{QW}}\sigma\sum_{=\uparrow,\downarrow}\sum_{nm}J_{cv}^{nm}\int_0^{+\infty}\rho_{2D}\left|M_{cv}\right|^2\left[f\left(E_{n,k}^{c}-E_F^{c}\right)-f\left(E_F^{v}-E_{m,k}^{v}\right)\right]\times \frac{\hbar/\tau_{in}}{\left(\hbar\omega-(E_{n,k}^{c}-E_{m,k}^{v})-E\right)^2+\left(\hbar/\tau_{in}\right)^2}dE$$

Where τin represents the intra-band relaxation time, equal to 10^{-13} s [18], e is the electron charge, c is the speed of light, ε_o is the vacuum permittivity, nr is the refractive index, LQw is the quantum well width, and m_o is the electron rest mass.

Results and Discussions

To analyze the impact of the quantum well (QW) width and α-Sn concentration on the subband structure and optical gain along the [110] and [111] directions, we calculated the dispersion relation of the conduction band (CB) and valence band (VB) subbands of Ge/Ge_{1-x} Sn_x/Ge quantum wells as a function of α-Sn concentration and well width. The necessary parameters for Ge and α-Sn, used in the numerical calculations, are provided in Table 1 of reference [18]. The well and barrier widths vary between (8, 10) nm and 12 nm, for α-Sn concentrations ranging from 0.08 to 0.185, and the confinement energy of the well is approximately 130 meV for heavy-hole HH_n and light-hole LH_n states [20]. It should be noted that the energy unit used is meV, and the reference energy is chosen at the highest level of the unstrained HH_n well. All the numerical parameters for bulk Ge and α-Sn used in this study are taken from references [9, 10].

Figure 2 illustrates the subband structure of the CB and VB of a single quantum well, for different well widths (8, 10) nm and 12 nm, as well as for various α-Sn concentrations (0.1, 0.16, and 0.18).The dispersions are shown along the crystallographic directions [110] and [111], represented by solid and dashed lines, respectively.

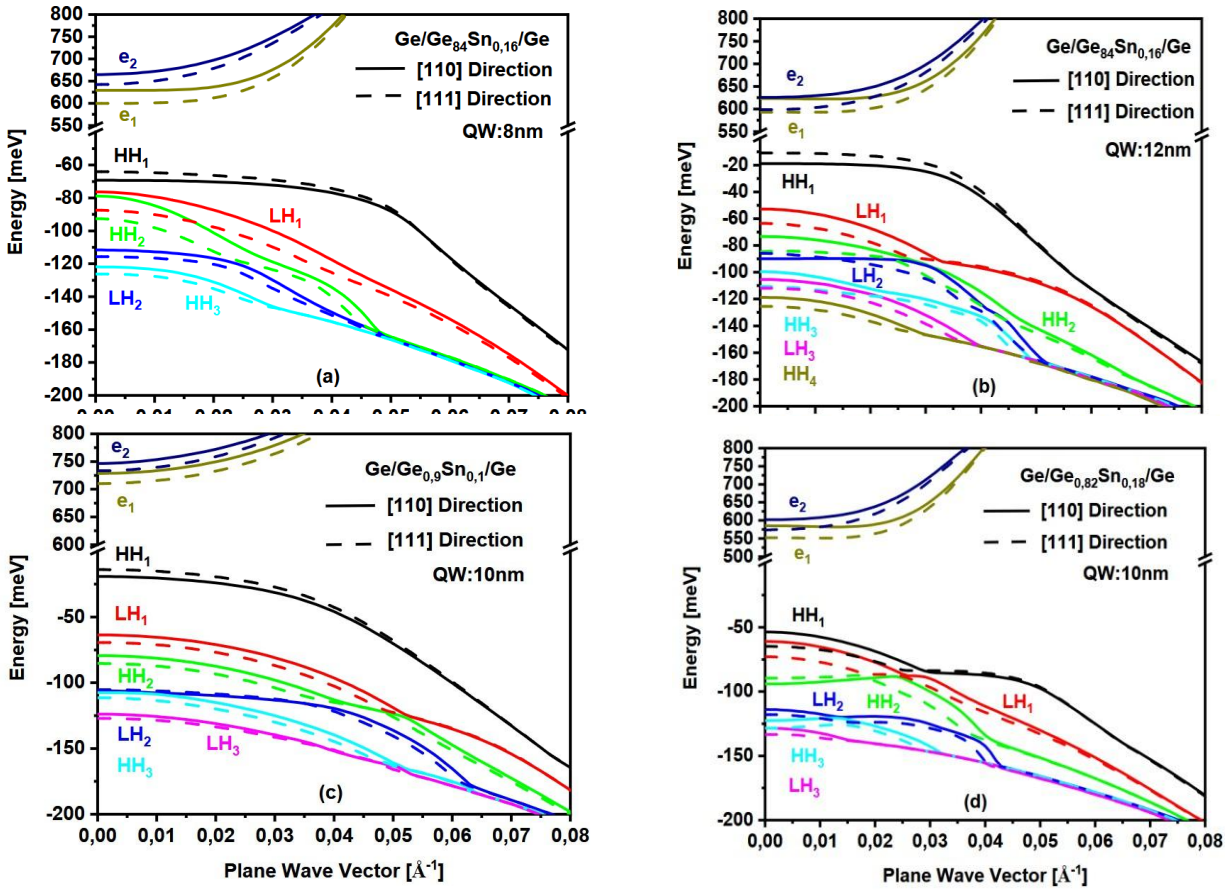

ISSN: 1737-9

Figure 2. CB and VB subband structure of the Ge/Ge_{1-x} Sn_x /Ge quantum well calculated for different α-Sn compositions (0.1, 0.16, and 0.18) and different quantum well thicknesses (8, 10, and 12 nm) along the crystallographic directions [110] and [111].

The confined hole- and electron- subband- states in the CB and VB are denoted by HH_n, LH_n, and e_n.
A clear anisotropy is observed between the [110] and [111] directions. This is manifested by a difference in the curvature of the conduction bands (e_1, e_2) and the valence subbands (HH_1, LH_1, etc.). The effect is particularly pronounced on the valence subbands, which exhibit strong coupling between heavy and light bands. By comparing Figure 2(a) to Figure 2(b), a reduction in the confinement energy of electrons and holes in the thicker structure is observed. This results in a progressive downward shift of the e_1/e_2 levels towards lower energies and a convergence of the HH_1/LH_1 levels towards zero. This reduction is more pronounced in the [110] direction. The dispersion difference between [110] and [111] becomes more noticeable, especially in the higher subbands.
In the [110] direction, the curves are slightly more inclined around k=0, particularly for the HH_1, LH_1 subbands, etc. This indicates a lower effective mass, hence more mobile carriers in this direction.
In the [111] direction, the curves are somewhat flatter around k=0, suggesting a larger effective mass, thus less mobile carriers. The energy levels are also less dispersed, reflecting stronger confinement in this direction. The dispersion differences between the [110] and [111] directions become more pronounced with increasing well width, especially for the higher levels. It is also noted that the difference between [110] and [111] is less marked for the electron levels compared to the hole levels. This indicates that electrons are more confined than holes in this structure. With Figures 2(c) and 2(d), it is observed that the Sn content strongly influences the band structure in both directions studied, with the coupling between subbands becoming more pronounced at higher concentrations.
Figures 3a and 3b illustrate the optical gain emission in the [110] and [111] directions as a function of quantum width (8, 10, 12, and 14 nm) and α-Sn concentration (0.08, 0.1, 0.12, 0.161, 0.18, and 0.185), for a typical injected carrier density (1.5×10^{19} cm^{-3}) in the Ge/$Ge_{1-x}Sn_x$/Ge structure.

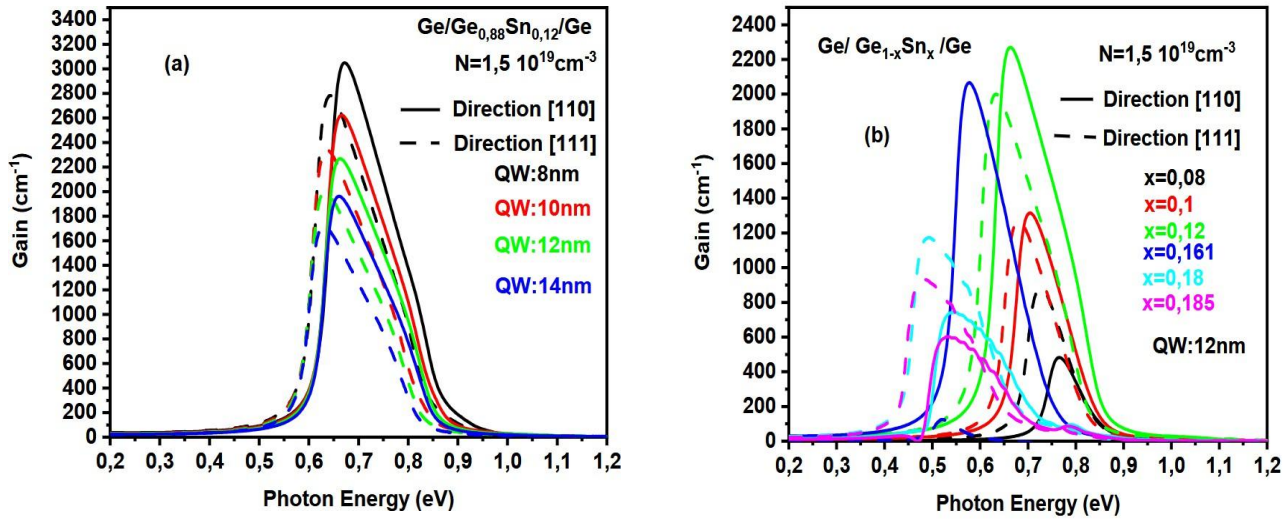

Figures 3. Optical gain emission along the [110] and [111] directions as a function of quantum well width (8–14 nm) and α-Sn content (0.08–0.185), at an injected carrier density of 1.5×10^{19} cm^{-3} in the Ge/$Ge_{1-x}Sn_x$/Ge structure.

As shown in Figure 3a, the maximum gain is generally higher for the narrower quantum wells, and this trend is observed in both crystallographic directions studied. Moreover, the [110] direction is typically more favorable in terms of optical performance.
Figure 3b demonstrates that at low Sn concentrations (x = 0.08), the maximum gain — i.e., the peak — is more pronounced in the [111] direction compared to the [110] direction. However, as the

ISSN: 1737-9334

concentration increases to x = 0.16, this trend reverses, with the [110] direction showing a higher gain. Beyond this concentration (x > 0.16), the initial behavior is restored, with the gain peak again higher in the [111] direction. Moreover, the crystallographic directions influence the curves in a similar manner, except for an α-Sn concentration of 0.161, where the gain in the [111] direction decreases drastically.

Conclusions

We have emphasized that the crystallographic directions influence the curves in a similar manner, although the differences between the [110] and [111] directions highlight the material's anisotropy, slightly modifying the transition energy and gain amplitude. We also noted that the effect of Sn appears to be a more significant factor than quantum well width in modulating optical gain. Furthermore, it should be noted that the [110] direction generally proves to be more favorable in terms of optical performance. In our study, by maintaining a constant carrier density, we highlighted the direct impact of geometric parameters on the gain behavior. This approach allows for the separation of effects related to quantum well engineering from doping effects, which is crucial for experimental design.

References

[1] A. Georgakilas, J. Stoemenos, K. Tsagaraki, P. Komninou, N. Flevaris, P. Panayotatos, and A. Christou, “Generation and annihilation of antiphase domain boundaries in GaAs on Si grown by molecular beam epitaxy,” J. Mater. Res. **8**(08), 1908–1921 (1993).

[2] A Ben Ahmed1, S Ridene, M Debbichi, M Sa¨ıd and H Bouchriha, Semicond. Sci. Technol. 28 (2013) 065006 (10pp). Online at stacks.iop.org/SST/28/065006

[3] Y. Bogumilowicz, J. M. Hartmann, R. Cipro, R. Alcotte, M. Martin, F. Bassani, J. Moeyaert, T. Baron, J. B. Pin,X. Bao, Z. Ye, and E. Sanchez, “Anti-phase boundaries–Free GaAs epilayers on “quasi-nominal” Ge-buffered silicon substrates,” Appl. Phys. Lett. **107**(21), 212105 (2015).

[4] D. Zubia and S. D. Hersee, “Nanoheteroepitaxy: The Application of nanostructuring and substrate compliance to the heteroepitaxy of mismatched semiconductor materials,” J. Appl. Phys. **85**(9), 6492–6496 (1999).

[5] J. Z. Li, J. Bai, C. Major, M. Carroll, A. Lochtefeld, and Z. Shellenbarger, “Defect reduction of GaAs/Si epitaxy by aspect ratio trapping,” J. Appl. Phys. **103**(10), 106102 (2008).

[6] H. Schmid, M. Borg, K. Moselund, L. Gignac, C. M. Breslin, J. Bruley, D. Cutaia, and H. Riel, “Template- assisted selective epitaxy of III–V nanoscale devices for co-planar heterogeneous integration with Si,” Appl. Phys. Lett. **106**(23), 233101 (2015).

[7] M. Knoedler, N. Bologna, H. Schmid, M. Borg, K. Moselund, S. Wirths, M. D. Rossell, and H. Riel, “Observation of Twin-free GaAs Nanowire Growth Using Template-Assisted Selective Epitaxy,” Cryst. Growth. Res. **17**(12), 6297–6302 (2017).

[8] J. Liu, X. Sun, D. Pan, X. Wang, L. C. Kimerling, T. L. Koch, and J. Michel, “Tensile-strained, n-type Ge as a gain medium for monolithic laser integration on Si,” Opt. Express **15**(18), 11272–11277 (2007).

[9] Zitouni. O, Saidi. H, Ridene. S. Investigation of α-Sn Dependence of Band Structure and Optical Emission in $Si/Si_yGe_{1-x-y}Sn_x/Si$ Quantum Well Laser. *Silicon* 2024, 16, 3573–3581. https://doi.org/10.1007/s12633-024-02928-7

[10] Chen. Z, Ikonic. Z, Indjin. D, Kelsall. R.W. Design optimization of tensile-strained SiGeSn/GeSn quantum wells at room temperature. J. Appl. Phys.2021, 129, 123102. https://doi.org/10.1063/5.0042482

[11] Asada. M, A.K. Ama. A.K, Suematsu. Y. Gain and intervalence band absorption in quantum-well lasers. IEEE J. Quantum Electron. 1984, 20, 745–753. https://doi.org/10.1109/JQE.1984.1072464

[12] A. Gassenq, K. Guilloy, G. Osvaldo-Dias, N. Pauc, D. Rouchon, J. M. Hartmann, J. Widiez, S. Tardif, F. Rieutord, J. Escalante, I. Duchemin, Y.-M. Niquet, R. Geiger, T. Zabel, H. Sigg, J. Faist, A. Chelnokov, V.

ISSN: 1737-9334

Reboud, and V. Calvo, "1.9% bi-axial tensile strain in thick germanium suspended membranes fabricated in optical germanium-on-insulator substrates for laser applications," Appl. Phys. Lett. **107**(19), 191904 (2015).

[13] S. Wirths, R. Geiger, N. von den Driesch, G. Mussler, T. Stoica, S. Mantl, Z. Ikonic, M. Luysberg, S. Chiussi, J.M. Hartmann, H. Sigg, J. Faist, D. Buca, and D. Grutzmacher, "Lasing in direct-bandgap GeSn alloy grown on Si," Nat. Photonics **9**(2), 88–92 (2015).

[14] D. Stange, N. von den Driesch, D. Rainko, T. Zabel, and B. Marzban, Z. ikonic, P. Zaumseil, G. Capellini, S. Mantl, J. Witzens, H. Sigg, D. Grutzmacher, and D. Buca "Quantum Confinement Effects in GeSn/SiGeSn Heterostructure Lasers," in *2017 IEEE International Electron Devices Meeting* (2017), paper 24.2.1.

ISSN: 1737-9334